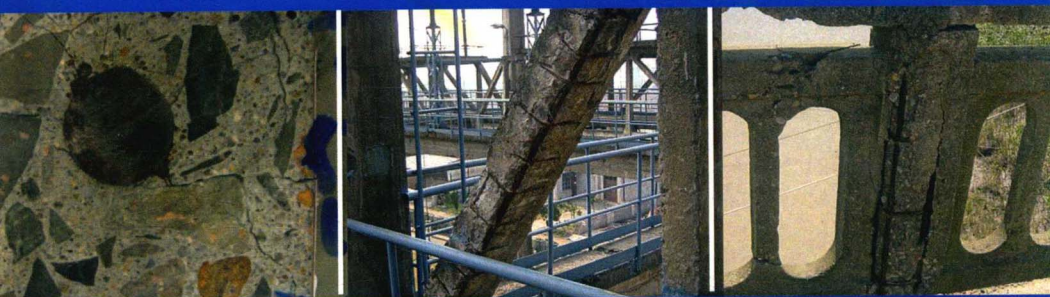


STEEL CORROSION-INDUCED CONCRETE CRACKING

钢筋锈蚀引起的混凝土开裂



Yuxi Zhao
Weiliang Jin



科学出版社

Steel Corrosion-Induced Concrete Cracking

钢筋锈蚀引起的混凝土开裂

Yuxi Zhao

Zhejiang University, Hangzhou, China

Weiliang Jin

Zhejiang University, Hangzhou, China



Butterworth-Heinemann
An imprint of Elsevier
elsevier.com



Science Press
Beijing

Copyright ©2016 China Science Publishing & Media Ltd. All rights reserved.

No part of this publication may be reproduced or ~~transmitted in any form~~ or by any means, electronic or mechanical, including photocopying, recording, or ~~any information storage~~ and retrieval system, without permission in writing from the publisher.

This book and the individual contributions contained in it are protected under copyright by the Publisher (other than as may be noted herein).

Not for sale outside the Mainland of China (Not for sale in Hong Kong SAR, Macau SAR, and Taiwan, and all countries, except the Mainland of China).

Notices

Knowledge and best practice in this field are constantly changing. As new research and experience broaden our understanding, changes in research methods, professional practices, or medical treatment may become necessary.

Practitioners and researchers must always rely on their own experience and knowledge in evaluating and using any information, methods, compounds, or experiments described herein. In using such information or methods they should be mindful of their own safety and the safety of others, including parties for whom they have a professional responsibility.

To the fullest extent of the law, neither the Publisher nor the authors, contributors, or editors, assume any liability for any injury and/or damage to persons or property as a matter of products liability, negligence or otherwise, or from any use or operation of any methods, products, instructions, or ideas contained in the material herein.

ISBN: 978-7-03-047437-7

Science Press, Beijing

ISBN: 978-0-12-809197-5

Butterworth-Heinemann, an imprint of Elsevier

Published by Science Press

16 Donghuangchenggen North Street

Beijing 100717, P.R.China

Printed in Beijing

Foreword

Service life of unreinforced concrete structures can be extremely long. Many historical structures from the Roman period demonstrate this fact convincingly, such as the Pantheon in Rome, which is built of high-strength concrete, normal concrete, and a cupola of extremely lightweight concrete, or Roman bridges all over Europe. They have survived thousands of years under the effects of natural exposure, wars, and earthquakes without protection or maintenance.

If steel reinforcement is embedded in concrete, then the steel is protected initially by a surface passivation layer in the aqueous pore solution because of its high pH value. This passivation layer, however, is not stable in aging concrete. Concrete is a porous material. At first, the pore space is partially filled with water and is in equilibrium with high relative humidity. However, the surface of reinforced concrete structures is often exposed to an atmosphere with much lower humidity. As a consequence, a long-lasting drying process begins as soon as the formwork is removed. As the pore space is partially emptied, gases diluted in the surrounding air such as CO_2 will slowly migrate into the pore space and react with the young cement-based matrix. First, a thin layer of carbonated hydration products is formed near the surface. When the growing thickness of this carbonated layer reaches the cover thickness, the pH value of the pore liquid in contact with the steel reinforcement is lowered and the protective passivation layer is eventually destroyed. Hence, corrosion is initiated.

If the surface of concrete is temporarily in contact with an aqueous chloride solution such as sea water or water containing dissolved deicing salt, then chloride ions can penetrate into the pore space of the concrete. Fortunately, the chloride ions are filtered out of the salt solution and they are enriched close to the surface; however, the clean water may penetrate deep into the pore space by capillary action. Later, dissolved chloride ions migrate deeper into the nanoporous material by slow diffusion. Whenever the chloride concentration near the steel reinforcement reaches a critical value, the protective passivation layer may be locally destroyed and corrosion of steel begins.

Until now, durability design had not reached the sophisticated level of structural design. Usually one considers different stages, for instance, corrosion initiation, crack formation, and spalling. After initiation, the rate of

corrosion may be rather low. But after the first cracks are generated, corrosion will be significantly accelerated. The authors of this book primarily describe the formation of corrosion products and the time-dependent pressure built up by the voluminous corrosion products. These are essential processes that may serve as indications of the end of service life of reinforced concrete structures.

The mechanisms of steel corrosion in concrete are briefly described. The following chapters describe in great detail the formation of corrosion products at the interface between steel and concrete. In particular, the gradual filling of the pores of hardened cement paste and the gradual filling of cracks with corrosion products are considered. Finally, a model describing concrete cracking due to the formation of corrosion products is presented. This approach and the results obtained by the two authors of this book will be very helpful for more realistic prediction of the service life of reinforced concrete structures.

In this book, the complex processes that can be observed during the critical period of aging concrete between corrosion initiation and crack formation in the concrete cover and then, finally, spalling of the layer near the surface are described in great detail for the first time. A better understanding of these complex processes will contribute to the development of more reliable prediction of service life and of more efficient methods for protective interventions. Therefore, the service life of reinforced concrete structures can be extended systematically and the cost of repair measures can be substantially reduced. This is of particular importance for countries like China, in which a nationwide infrastructure is rapidly being built. In no other country is more concrete being produced at this moment.

If modern construction does not become more sustainable, and if the service life of reinforced concrete structures is not significantly extended, then further development will be slowed because of the enormous costs for repair and maintenance of the existing infrastructure. This book may contribute a great deal to finding realistic and sustainable solutions to this worldwide problem.

This volume deserves wide distribution and will hopefully be studied in great detail by scientists and practitioners. With this book, the actual situation concerning durability and service life in construction can be improved substantially worldwide.

Folker H. Wittmann

Preface

Since the mid 1970s, a number of durability-related problems have emerged and stimulated research of the key factors that relate to the durability problems of concrete structures. Reinforcing steel corrosion is one of the major reasons for deterioration of reinforced concrete structures. Steel corrosion in concrete will induce sectional loss of steel bar, degradation of bond stress between steel and concrete, and cracks parallel to longitudinal bars. Field studies have suggested that cracking and spalling are most concerning to asset owners. Structural collapse of reinforced concrete structures due to steel corrosion is rare; cracking, rust staining, and spalling of the concrete cover usually appear well before a reinforced concrete structure is at risk. Therefore, the cracking of the concrete cover induced by steel corrosion is important and is usually defined as the serviceability limit state.

The authors have focused on this research field since 1998, and have carefully investigated the origin, mechanism, and development of corrosion-induced cracking in concrete. Considering the importance of this topic, the authors summarize the related research achievements obtained and share with other researchers and engineers who are interested in this field. This book concentrates on the concrete cracking process induced by steel corrosion. After the background introduction and literature review in chapter "Introduction," the mechanisms of steel corrosion in concrete are introduced in chapter "Steel Corrosion in Concrete." The composition, expansion coefficient, and elastic modulus of steel corrosion are carefully investigated in chapter "The Expansion Coefficients and Modulus of Steel Corrosion Products," considering the importance of the properties of steel corrosion in concrete cracking models. With these parameters of steel corrosion, the damage analysis is applied to analyze the corrosion-induced concrete cracking process in chapter "Damage Analysis and Cracking Model of Reinforced Concrete Structures With Rebar Corrosion," and the critical thickness of the rust layer at the moment of surface cracking of concrete cover is studied in chapter "Mill Scale and Corrosion Layer at Concrete Surface Cracking." In chapter "Rust Distribution in Corrosion-Induced Cracking Concrete," the authors investigate the rust distribution in the corrosion-induced cracks and find that the rust did not fill the corrosion-induced cracks in the concrete cover before concrete surface cracking. A Gaussian function is proposed to describe the nonuniform spatial distribution of corrosion products in chapter

"Nonuniform Distribution of Rust Layer Around Steel Bar in Concrete." The shape of the corrosion-induced cracks in the concrete cover is observed in chapter "Crack Shape of Corrosion-Induced Cracking in the Concrete Cover," and a linear model was proposed to describe the variation in the total circumferential crack width along the radial direction in the concrete cover. Rust distribution at the steel-concrete interface is presented in chapter "Development of Corrosion Products-Filled Paste at the Steel-Concrete Interface"; and the penetration of corrosion products into the porous zone of concrete and formation of a corrosion layer at the steel-concrete interface process simultaneously. Finally, in chapter "Steel Corrosion-Induced Concrete Cracking Model," an improved corrosion-induced cracking model is proposed, which considers the corrosion layer accumulation and corrosion products filling occurring simultaneously in concrete. The time from corrosion initiation to concrete surface cracking is discussed. The need for more research regarding the corrosion-induced cracking model is also discussed in this book.

The authors hope this book is useful for researchers interested in the durability of concrete and concrete structure fields, for industry engineers who pay attention to the deterioration mechanisms and the life cycle of reinforced concrete structures, and for graduate students whose research topics include corrosion-induced deterioration of reinforced concrete structures.

Acknowledgments

Continuous financial support from the National Science Foundation of China (NSFC) through grants 50538070, 50920105806, 50808157, and 51278460 is gratefully acknowledged. Without this financial support, it would be not possible to perform all the experimental work, develop the analytical models, and further the research in this area.

The authors also express sincere gratitude to the graduate students who contributed their talent, intelligence, effort, and hard work to this research. They are Haiyang Ren, Jiang Yu, Bingyan Hu, Hong Dai, Yingyao Wu, Hangjie Ding, Jianfeng Dong, and Xiaowen Zhang. Particular thanks are expressed to Hangjie Ding, Jianfeng Dong, and Xiaowen Zhang, who also helped to edit the contents, improve the format, and modify some figures in this book.

We appreciate the comments and encouragement from Professor Folker H. Wittmann, his comments improve the quality of the book, he also kindly wrote the *Foreword*. Many thanks to the reviewers of this book for their time. Their helpful suggestions have strengthened the book considerably. Our thanks also go to the publisher and the editor Fanjie Wu, who patiently replied to all our questions and helped us as much as possible.

We apologize for naming such a small number of the many people who helped us and with whom we had the pleasure of working. Sincere thanks to all of them for their willingness to share their knowledge with us and for encouraging us to go further and further in this area.

List of Figures

Figure 1.1	Comparison of steel corrosion at concrete surface cracking between the empirical model-predicted results and the experimental results.	6
Figure 1.2	Comparison of concrete surface crack width propagation between the model-predicted results and the experimental results.	7
Figure 1.3	Three-stage corrosion-induced cracking process. (a) Corrosion initiated. (b) Stage 1: filling. (c) Stage 2: stressing. (d) Stage 3: cracking.	8
Figure 1.4	BSE images showing accumulation of corrosion products at the steel–concrete interface (S, steel; CL, corrosion layer; CP, corrosion products-filled paste; P, unaltered paste; A, air void).	9
Figure 1.5	Corrosion-induced concrete cracking model. (a) Thick-walled cylinder model. (b) Double-layer thick-walled cylinder model.	12
Figure 2.1	The anodic and cathodic reactions.	20
Figure 2.2	Initiation and propagation periods for steel corrosion in concrete.	23
Figure 2.3	Pitting attack in a steel bar.	24
Figure 2.4	Transformation of iron oxides.	27
Figure 2.5	Stages in corrosion-induced damage. (a) Passive rebar. (b) Corrosion initiation and growth. (c) Further corrosion and cracking propagation. (d) Spalling/delamination.	28
Figure 3.1	XRD pattern of eight different rust samples.	36
Figure 3.2	TG curves of all rust samples.	37
Figure 3.3	DTA curves of all rust samples.	38
Figure 3.4	XRD patterns of the original and heated sample 1.	40
Figure 3.5	Improved XRD patterns of eight rust samples.	41
Figure 3.6	The concrete port and the steel corrosion products. (a) The concrete port in Yokosuka. (b) The corroded steel bar in the concrete beam. (c) The corrosion product peeled from the corroded steel bar. (d) Flaky rust samples.	47

Figure 3.7	Typical loading and unloading stress–strain curve.	48
Figure 4.1	Deformations of the rust layer and surrounding concrete under expansive pressure. (a) Noncracking. (b) Partial cracking.	57
Figure 4.2	Partitions of the cracking part.	63
Figure 4.3	Expansive pressure against steel corrosion.	67
Figure 4.4	Variation of expansive pressure after initiation of cracks in concrete cover. (a) Expansive pressure against crack length. (b) Expansive pressure in cracked concrete.	68
Figure 4.5	Effect of concrete cover thickness on expansive pressure.	69
Figure 4.6	Peak value of expansive pressure against concrete cover thickness.	69
Figure 4.7	Normalized expansive pressure as a function of normalized crack length.	70
Figure 4.8	Effect of steel bar diameter on expansive pressure.	71
Figure 4.9	Effect of tensile strength on expansive pressure.	72
Figure 4.10	Radial loss of steel bar as a function of crack length.	73
Figure 4.11	Effect of concrete cover thickness on steel loss during surface cracking.	74
Figure 4.12	Effect of steel bar diameter on steel loss during surface cracking.	74
Figure 4.13	Effect of rust expansion coefficient on steel loss during surface cracking.	75
Figure 4.14	Effect of compressive strength on steel loss during surface cracking.	76
Figure 5.1	Layout details of the concrete specimens (dimensions are in mm).	80
Figure 5.2	Cracking parts of specimens were cast into a low-viscosity epoxy resin.	81
Figure 5.3	Schematic diagrams of the specimens and the location of the slices.	82
Figure 5.4	Sample (slice 1-1) for digital microscope observation.	82
Figure 5.5	Sample trimmed from slice 2-2 for SEM observation.	83
Figure 5.6	Rust distributions at the steel–concrete interface and in the corrosion-induced cracks (<i>CP</i> , corrosion products-filled paste; <i>CL</i> , corrosion layer).	84

Figure 5.7	EDS analysis across a corrosion-induced crack. (a) Corrosion-induced crack and an analytical line across the crack. (b) Distribution of Fe across the corrosion-induced crack analyzed by EDS along the analytical line.	85
Figure 5.8	EDS analysis across the steel–concrete interface. (a) BSE image at the steel–concrete interface (MS, mill scale) and an analytical line across the interface. (b) The distribution of Fe and O across the steel–concrete interface analyzed by EDS along the analytical line.	86
Figure 5.9	Mill scale distribution at the steel–concrete interface.	87
Figure 5.10	Crack pattern of slice 1-1.	88
Figure 5.11	Crack pattern of slice 2-1.	89
Figure 5.12	The crack patterns on the cross-section of the measured slices. The longest radial crack length and the corrosion layer thickness are listed below each slice.	90
Figure 5.13	Relation between corrosion layer thickness and crack length.	91
Figure 6.1	Schematic of the reinforced concrete specimen (dimensions are in mm).	94
Figure 6.2	Schematic diagrams of the cut specimen. (a) Specimen. (b) The cut panels and slices.	95
Figure 6.3	Sample preparation for SEM. (a) Slice L-9. (b) Sample for SEM.	96
Figure 6.4	Measurement of the thickness of the rust layer accumulated at the rebar–concrete interface. (a) Field of view: 50×52 mm. (b) Field of view: 3.74 × 3.68 mm.	97
Figure 6.5	Rust distributions at the steel–concrete interface in sample R-5. (a) BSE image at the steel–concrete interface (CP, corrosion products-filled paste; MS, mill scale; CL, corrosion layer) and an analytical line across the interface. (b) The distributions of Fe and O across the steel–concrete interface analyzed by EDS along the analytical line.	98
Figure 6.6	Schematic of ion migration and reaction during steel corrosion in the presence of chloride ions in concrete.	99

Figure 6.7	Average thickness of the corrosion products-filled paste (CP) for different thicknesses of the corrosion layer (CL).	100
Figure 6.8	Rust distribution in slice R-6. (a) Slice R-6. (b) Area 1. (c) Area 2. (d) Area 3. (e) Area 4.	102
Figure 6.9	Crack at the steel-concrete interface of slice M-14 ($6897\mu\text{m} \times 6155\mu\text{m}$).	103
Figure 6.10	Slice L-4 with the more severe corroded steel bar.	104
Figure 6.11	Rust distributed in a crack penetrating the concrete cover in sample L-9. (a) BSE image of the corrosion-induced crack and an analytical line across the crack. (b) The distribution of Fe across the crack analyzed by EDS along the analytical line.	105
Figure 6.12	Rust distributed in an inner crack in sample R-7. (a) BSE image of the corrosion-induced crack and an analytical line across the crack. (b) The distribution of Fe across the crack analyzed by EDS along the analytical line.	106
Figure 6.13	Schematic diagram of crack propagation and rust development. (a) Before surface cracking. (b) Surface cracking. (c) After surface cracking.	107
Figure 7.1	Steel corrosion varies with the distance to the front of specimen R.	112
Figure 7.2	Typical cracks and rust layer of slices from specimen R.	113
Figure 7.3	Measured thickness of the rust layer around the rebar perimeter.	114
Figure 7.4	Polar coordinate system defined for the corner and middle rebars.	115
Figure 7.5	Polar coordinate system for measurement and fitting of the rust layer.	117
Figure 7.6	The regression analysis of the proposed models for the tested data.	119
Figure 7.7	R^2 of four models.	120
Figure 7.8	Physical meaning of λ_3 . (a) Partial corrosion ($\lambda_3 = 0$). (b) Whole cross-section corrosion ($\lambda_3 = T_{r,\min}$).	120
Figure 7.9	Two parts of the rust layer when steel corrosion spreads throughout the entire circumference.	122
Figure 7.10	Area of corrosion peaks grow with the increase of λ_1 .	122
Figure 7.11	Peak area of partial corrosion.	123
Figure 7.12	Relationship between λ_1 and ρ .	123

Figure 7.13	Nonuniform corrosion spreading widely with the increase of λ_2 .	124
Figure 8.1	Layout details of specimens (dimensions are in mm).	130
Figure 8.2	Wetting and drying cycles combined with a constant current.	131
Figure 8.3	Schematic diagram of preparation of samples for digital microscopy observation. (a) Cracked parts of specimens were cast in epoxy resin. (b) A sample prepared for digital microscopy observation.	132
Figure 8.4	Measurement and calculation of the crack width, W_i , at radius R_i . (a) Measurement of crack width. (b) Total crack width, W_i .	133
Figure 8.5	Measured data and the fitting line of the crack width. (a) Slice R000-1-8, representing the inner cracking scenario. (b) Slice R000-2-8, representing the cracks that had penetrated the concrete cover.	135
Figure 8.6	Schematic crack shape model.	136
Figure 8.7	Relationship between parameter a_1 and corrosion layer thickness T_{CL} .	137
Figure 8.8	Relationship between parameter a_2 and corrosion layer thickness T_{CL} .	138
Figure 8.9	Relationship between crack width on concrete surface, W_s , and corrosion layer thickness, T_{CL} .	141
Figure 8.10	Schematic diagram of corrosion-induced crack propagation.	142
Figure 9.1	Influence of cracks on CP development. (a–c) Inner crack. (d, e) Outer crack. CP, corrosion products-filled paste; CL, corrosion layer; T_{CP} , thickness of CP; T_{CL} , thickness of CL.	148
Figure 9.2	Schematic of measured regions at the concrete–steel interface.	150
Figure 9.3	Thickness of the corrosion products-filled paste (CP) versus thicknesses of the corrosion layer (CL) excluding the regions of the inner cracks for R000. (a) Measured data. (b) A part of the data map after grouping in the range of 20 μm for R067.	150
Figure 9.4	Relationship between T_{CP} and T_{CL} excluding the regions of the inner cracks. (a) R000. (b) R033. (c) R067. (d) R100.	151
Figure 9.5	$T_{CP}-T_{CL}$ models for four types of concrete (excluding the effect of inner cracks).	152
Figure 9.6	Effect of concrete quality on T_{CP} .	152

Figure 9.7	Thickness of corrosion products-filled paste (CP) versus thickness of corrosion layer (CL) including the regions of the inner crack for R000s. (a) All measured data. (b) Local magnification.	153
Figure 9.8	Tested data of all samples and their average value of tested data.	156
Figure 9.9	T_{CP} – T_{CL} models for four types of concrete (including the effect of inner cracks). CP, corrosion products-filled paste; T_{CP} , thickness of CP; T_{CL} , thickness of corrosion layer.	156
Figure 10.1	Corrosion-induced concrete cracking model considering corrosion products-filled paste. (a) Steel depassivation. (b) Corrosion-induced crack appears and CP and CL form simultaneously. (c) T_{CL} and T_{CP} increase gradually until the crack reaches the concrete outer surface.	160
Figure 10.2	Relationship between T_{CP} and T_{CL} .	161
Figure 10.3	Conversion from the thickness of CP (T_{CP}) to the thickness of CL ($T_{CL,pore}$).	162
Figure 10.4	Nonuniform corrosion layer and the corresponding CP thickness. (a) Nonuniform corrosion layer. (b) Corresponding CP thickness.	168
Figure 10.5	The mechanical interlocking between the steel ribs and the concrete keys.	169

List of Tables

Table 1.1	Experimental Study of Corrosion Products-Filled Paste	9
Table 1.2	Corrosion-Induced Cracking Model	11
Table 1.3	Rust Filling in Corrosion-Induced Cracks	13
Table 2.1	Different Types of Iron Oxides	25
Table 2.2	Selected Properties of the Iron Oxides	27
Table 3.1	Details of the Rust Samples	34
Table 3.2	The Content of Two Categories: Products for Eight Samples (mg)	42
Table 3.3	The Expansion Coefficient of the Main Hydroxy-Oxides and Oxides	43
Table 3.4	The Expansion Coefficients for All Rust Samples	44
Table 3.5	Exposure Classes Related to Environmental Conditions	44
Table 3.6	Environmental Classifications for All Rust Samples	45
Table 3.7	Rust Expansion Coefficients Corresponding to Different Environments	46
Table 3.8	Tested Data from the Cyclic Low-Compression Test	50
Table 4.1	Calculated Mechanical Parameters of the Four Types of Concrete	72
Table 5.1	Mixture Composition of the Concrete Specimens (kg/m ³)	80
Table 6.1	Mixture Composition of Concrete Specimens (kg/m ³)	94
Table 6.2	Data for Each Group in Fig. 6.7	101
Table 7.1	Values of λ_1 , λ_2 , λ_3 , and λ_4 Obtained from the Fitting of Experimental Data	115
Table 7.2	Description of Two Nonuniform Corrosion Scenarios	116
Table 7.3	Parametric Regression Value in Model	118
Table 8.1	Compositions of the Concrete Specimen Mixtures	130
Table 8.2	Measurement Results and Parametric Regression Values	136
Table 8.3	Linear Regression Results for a_1 Compared to T_{CL}	138
Table 8.4	Linear Regression Results for a_2 Compared to T_{CL}	139
Table 8.5	Substituting Results of W_i and Critical Crack Width W_c	139
Table 8.6	Linear Regression Results of W_s Compared to T_{CL}	141
Table 8.7	Comparison of Crack Shapes Between NAC and RAC	144

Table 9.1	Fitting Values of k_T and T_{CP}^{max} (μm)	151
Table 9.2	Average T_{CP} and T_{CL} of Each Sample, Mean Values of T_{CP} , and Their Mean Square Deviation of Each Type of Concrete Specimens (μm)	155
Table 9.3	Values of k_T Considering the Effect of Inner Cracks	156

Contents

Foreword	xi
Preface	xiii
Acknowledgments	xv
List of Figures	xvii
List of Tables	xxiii
1. Introduction	1
1.1 Background	1
1.2 Empirical Models	2
1.2.1 Critical Steel Corrosion at Surface Cracking	2
1.2.2 Crack Width at the Concrete Surface	4
1.2.3 Discussion on the Empirical Models	6
1.3 Analytical Models	7
1.3.1 Three-Stage Corrosion-Induced Cracking Model	7
1.3.2 Corrosion Products Filling Stage	8
1.3.3 Concrete Cover Stressing and Cracking	10
1.3.4 Rust Filling in Corrosion-Induced Cracks	13
1.4 Contents of This Book	13
References	15
2. Steel Corrosion in Concrete	19
2.1 Introduction	19
2.2 Mechanisms of Steel Corrosion in Concrete	20
2.2.1 Corrosion Process	20
2.2.2 Corrosion Rate	21
2.2.3 Passivation	21
2.3 Steel Corrosion Induced by Carbonation or Chloride Attack	22
2.3.1 Carbonation-Induced Corrosion	23
2.3.2 Chloride-Induced Corrosion	23
2.4 Corrosion Products	25
2.5 Steel Corrosion-Induced Concrete Damage	27
2.6 Conclusions	28
References	29